THE AMERICAN SOCIETY OF MECHANICAL ENGINEERS
345 E. 47 St., New York, N.Y. 10017

Airframe/Propulsion Integration at Transonic Speeds

WILLIAM P. HENDERSON
Applied Aerodynamics Division
NASA Langley Research Center
Hampton, Virginia

ABSTRACT

A significant level of research is ongoing at NASA's Langley Research center on integrating the propulsion system with the aircraft. This program has included nacelle/pylon/wing integration for turbofan transports, propeller/nacelle/wing integration for turboprop transports, and nozzle/afterbody/empennage integration for high performance aircraft. The studies included in this paper focus more specifically on pylon shaping and nacelle bypass ratio studies for turbofan transports, nacelle and wing contouring and propeller location effects for turboprop transports, empennage effects, and thrust vectoring for high performance aircraft. The studies were primarily conducted in NASA Langley's 16-Foot Transonic Tunnel at Mach numbers up to 1.20.

NOMENCLATURE

b	tail span
c	local chord
C_D	drag coefficient
C_L	lift coefficient
C_n	yawing moment coefficient
C_P	static pressure coefficient
C_T	thrust coefficient
D_n	nozzle drag
F	thrust
F_i	ideal thrust
H_T	horizontal tails
M	Mach number
NPR	nozzle pressure ratio
q	freestream dynamic pressure
V_T	vertical tail
x	distance from model nose along model centerline
y	distance spanwise from model centerline
z	model length
$\Delta C_{D,it}$	increment in drag coefficient due to interference effects
$\Delta C_{D_{N/P}}$	increment in drag coefficient due to nacelle/pylons
$\Delta C_{D_{\text{Tail}}}$	increment in drag due to horizontal and vertical tails
$\delta_{v,p}$	thrust deflection in pitch direction
$\delta_{v,y}$	thrust deflection in yaw direction

ABBREVIATIONS:

AFT	aft locations
Fwd	forward location
Stag	staggard location
L.E.	leading edge

INTRODUCTION

The interactions between the propulsion system and the airframe can have a significant impact on the performance of an advanced airplane design. These interactions are inherent in most designs particularly in those concepts where the inlet and nozzle are closely coupled or when the propulsion system is located close to a wing or to other aircraft components. It is not only very difficult to accurately predict these complex flow interactions, but it is also extremely difficult to develop the necessary experimental apparatus/models which can be utilized to develop a full understanding of the complex flow interactions, and to determine the impact of these interactions on the performance of advanced aircraft.

Over the last decade NASA Langley Research Center (LaRC) has been actively involved in developing the needed technology base for the effective integration of the propulsion system into a wide variety of aircraft concepts. The primary focus of attention has included the development and verification of innovative analytical methods for predicting airframe-propulsion interaction effects; the integration of inlet and nozzle concepts into advanced high performance aircraft designs; and the integration of high by-pass ratio turbofans or advanced high speed turboprops into the advanced transport aircraft.

This paper will present the results of several of these studies conducted by LaRC's Applied Aerodynamics Division which have contributed to the development of the needed technology base. This paper will concentrate on the integration of various aircraft components such as the engine nacelle/pylons and propeller/nacelles for turbofan and turboprop transports, respectively; and the integration of aircraft components such as the nozzle and empennage into high performance aircraft.

A vital part of any airframe/propulsion integration activity is the development and verification of computational methods that can be efficiently utilized in defining key experiments which will aid in the design process and in developing an understanding of the basic flow interactions. The results of several studies will be included in an attempt to define the benefit derived from the use of these advanced computational methods.

*Presented at the Gas Turbine and Aeroengine Congress and Exposition—June 11-14, 1990—Brussels, Belgium
This paper has been accepted for publication in the Transactions of the ASME
Discussion of it will be accepted at ASME Headquarters until September 30, 1990

DISCUSSION

The mission requirements for the next generation fighter aircraft may dictate a highly versatile vehicle capable of operating over a wide range of flight conditions. This aircraft will most likely be designed for high maneuverability and agility, operate in a highly hostile environment, and possess STOL landing characteristics to operate from bomb damaged airfields (1). Many design guidelines tend to be contradictory for the subsonic and supersonic speed regimes and aircraft performance can be compromised by small changes in these design considerations.

The attainment of high performance is highly dependent upon the minimization of interference resulting from the integration of the propulsion exhaust system into the airframe, one of the most critical design features of an aircraft (2). An indication of the relative importance of this area is illustrated in figure 1 where the percent of total aircraft drag attributed to the aircraft afterbody is presented for four twin-engine fighter aircraft. Representative aircraft form an "ideal" research configuration tested in 1961 to the F-18 aircraft tested in 1978 are shown. The afterbodies of these models comprised from 20 to 25 percent of the total model length, but produced 38 to 50 percent of the total aircraft drag. Up to half of this afterbody drag results from adverse interference in the afterbody region and pressure drag on the afterbody (3–9).

At the same time the designer is striving for a low drag configuration, he is also required to improve the maneuvering capability of the aircraft. This usually requires high thrust to weight and lift drag ratio, high useable lift coefficient, and adequate stability and control characteristics over a very wide operating envelope.

In responding to the need to reduce nozzle/afterbody drag and enhance vehicle maneuverability, the Propulsion Aerodynamics Branch at the Langley Research Center has conducted a number of responsive experimental and theoretical research programs.

In these studies it was found that one of the prime contributors to the high nozzle/afterbody drag is the empennage arrangement. A summary of the empennage effects on the single and twin engine models is present in figure 2 and discussed in reference 7. Empennage drag increments ratioed to total aft-end drag C_D are presented as a function of Mach number. The two data bands represent the range of data with varying vertical tail location when the horizontal tails are in the aft location. It is obvious from these data that empennage interference effects comprise a significant portion of the total aft-end drag, particularly in the high subsonic and transonic speed regime. It is also obvious that vertical tail location has a large impact on the magnitude of empennage interference. In the transonic speed regime empennage effects account for over half of the total aft-end drag depending upon vertical tail location and afterbody type. Based on the data of these figures couped with more detailed analysis, it is indicated that up to half of the total afterbody drag (afterbody, nozzle plus empennage) results form adverse interference on the nozzle/afterbody empennage configuration.

In an effort to address this critical area, NASA's Langley Research Center has undertaken a number of studies aimed at reducing the adverse interference drag on nozzle/afterbodies. The first research effort has been aimed at determining the effects of various empennage parameters on the aft-end drag and tail interference drag characteristics for twin engine (8) and for single-engine configurations (9) these studies were conducted in NASA Langley's 16-Foot Transonic Tunnel. Photographs of the single-engine tail interference afterbody model used in one of these studies is present in figure 3.

The overall model arrangement, representing a typical single-engine fighter aft end, is composed of four major parts located as shown in the following table:

Part	x, in.	x/l
Forebody	0–40.89	0–0.57
Afterbody	40.89–64.89	0.57–0.91
Nozzle	64.89–71.70	0.91–1.00
Tail Surfaces	Variable	Variable

The forebody consists of an ogive nose 24 in. in length with an initial angle of 14° and a constant-radius cylinder thereafter. The afterbody was designed to simulate closure ahead of the nozzle typical of a single- engine fighter configuration. The afterbody had provisions for mounting the vertical and horizontal tails at two different axial location (forward and aft). The tail surfaces were tested in three empennage arrangements: aft, staggered, and forward. Figure 4 illustrates the relative position of the tails for the three empennage arrangements. In addition, the model was tested with all tails removed. The nozzle used for this investigation simulated a variable geometry (fixed in dry power mode for this test), convergent-divergent, axisymmetric nozzle typical of those currently in use on modern fighter aircraft.

The effects of empennage arrangement on the total aft-end drag coefficient is presented in figure 5. The drag increments attributed to the nozzles, obtained by integrating surface pressures, and the horizontal and vertical tails, obtained by appropriate drag estimation procedures are also presented in this figure. At a Mach number of 0.95 the total drag decreases as the empennage is moved away from the nozzle. Moving the empennage appears to eliminate or reduce an adverse interference of the tails on the nozzle drag. However, moving the tails forward transfers some of this adverse interference to the afterbody. Note the magnitude of its open bar for the forward tail location as compared to the magnitude for its aft-tail configuration. Staggering the tail surfaces further reduces the drag of the aft-end of the configuration. This effect appears to result from a reduction in adverse interference on the afterbody which is larger than the increase in nozzle drag obtained as the horizontal tails are moved closer to the nozzle.

At a Mach number of 1.20 the lowest total aft-end drag is provided by the forward empennage arrangement. According to the data, the primary benefits results from a reduction in the nozzle drag as the tails are moved away from the nozzles.

The effects of empennage on the nozzle/afterbody pressure distribution (data taken from reference 11) is shown in figure 6. The circular symbols are the experimentally determined pressure distributions for the configuration with the empennage in the aft location. The dashed line is the experimental pressure distributions for the nozzle/afterbody with empennage off.

At the Mach number of 0.95, the empennage caused a large increase in velocities over the aft portion of the afterbody and forward portion of the nozzle ($x/l = 0.82$ to 0.92) which results in the formation of a shock wave at about $x/l = 0.92$ and flow separation over much of the nozzle (pressures on the nozzle are less positive than on the body alone). (See data for $\phi = 72°$ for example.) These high negative pressure coefficients acting on the rearward-facing projected area of the nozzle/afterbody along with the absence of pressure recovery on the nozzle (flow separation) cause the high level of interference drag.

It is of interest to note that the effects of the empennage are not limited to the regions close to the tail surface but extend completely around the nozzle/afterbody.

Eliminating these adverse interference effects will require the development of focused experimental and theoretical programs. NASA has spent considerable effort in this area and some of the results are shown in the next several figures. Several prediction methods for afterbody flow problems have been under study. One of the methods is a full-potential finite-volume

transonic code called FLO-30V (ref. 12), which is used to calculate the pressure distributions over the nozzle/afterbody including the effects of the empennage. In this code an integral boundary-layer calculation is performed in strip fashion. The resulting effective body and tails are used as input to the code. This developmental code utilizes the method of Caughey and Jameson which is based upon the full potential equation and a mesh generation technique which wraps a C-type grid around the body and tails.

The calculated results from the FLO-30V for the staggered empennage arrangement at subsonic speeds are compared with the experimental data in figure 7. The staggered tails arrangement was chosen because the results presented herein show that the empennage interference effects were less for this configuration than for the other configurations studied, and it is believed that a better agreement could be obtained. The calculated results show reasonably good agreement with the experimental data at the lowest test Mach number ($M = 0.60$). At the higher subsonic test Mach numbers, $M = 0.90$, the discrepancy between the experiment and theory becomes significant. The major reason for the discrepancy could probably be attributed to the approximations made to model the vertical tails and the lack of a model of the wake of the vertical tail. The FLO-30V calculations do account for viscous effects, but the boundary layers on the body and tail were computed separately as two-dimensional elements so that the influence of the empennage is not included in the afterbody boundary-layer calculations. As a result, the FLO-30V calculation shows some influence of the empennage on nozzle/afterbody pressures but fails to predict the severity of the interference effects at the higher Mach numbers.

One of the methods of reducing the nozzle/afterbody interference drag would be to reduce the size of the empennage. The effect of empennage size on the interference drag (measured drag increments removed from data) is presented in figure 8. In this figure the interference drag, $\Delta C_{D,it}$ is presented as a function of horizontal and vertical tail spans. The circular symbols are the data for the configuration with only the vertical tails, the square symbols are for the configuration with only the horizontal tails, and the diamond symbols are for the configuration with both the horizontal and vertical tails. Contrary to the expected result, the data of this figure indicate that most of the adverse tail interference ($\Delta C_{D,it}$) on the aft end is not caused by the portion of the tails closest to the afterbody but by the outer portion. For example, at $M = 0.95$, tail interference effects on the aft end were favorable (negative $\Delta C_{D,it}$) for y/b less than 0.16. For $M \leq 0.85$, however, tail interference effects were small or favorable for all tail arrangements when $y/b < 0.50$. These results indicate that it maybe possible to integrate a short-span surface such as a ventral fin with an increase in aft-end drag equal to or less than the drag on the surface itself.

If the horizontal and vertical tails are reduced in size or eliminated alternate methods of providing the necessary control power must be included. One method of providing the required control forces is through the utilization of thrust vectoring.

Methods of providing pitch vectoring have been under study for some time (reference 14). These studies have shown that many nozzles can be designed to provide high levels of pitch vectoring without a significant adverse impact on aircraft thrust performance. The challenge now becomes one of providing, in addition to the pitch vectoring, a high level of yaw vectoring. A number of configurational concepts have been studied and are shown in figure 9.

The upstream yaw vectoring concept was achieved by modifying one of the nozzle sidewalls with a rectangular port located upstream of the nozzle throat. The port was sized to have an area equal to 30 percent of the unvectored dry power nozzle throat area. The port operates by deflecting two flaps. The forward flap was a simple flap hinged at the nozzle sidewall and extended into the external flow. The aft flap was also hinged at the nozzle sidewall, but it deflected both into the external flow as well as into the internal flow (about 45 percent of the internal nozzle width). The flaps were deflected at an angle of about 70° to the axial thrust direction.

The downstream (of throat) yaw vectoring concept (sidewall flaps) is based on modifying either the left or right sidewall or both sidewalls with a hinged flap extending downstream of the nozzle throat. The sidewall flaps hinged directly at the nozzle throat. Consequently, for a positive yaw vector angle (produces positive side force), the left sidewall flap extends out from the internal nozzle flow (expansion turn), while the right sidewall flap extends into the flow (compression turn). This type of concept does have some limitations in that there would be some interference between surfaces when simultaneous pitch and yaw vectoring are required.

The third concept consisted of externally mounted vanes, one on each side of the nozzle. The vanes which are hinged at the nozzle exit are deflected such that one vane extends into the jet exhaust flow whereas the other extends away from the jet exhaust flow. The height of the vanes was determined by the location of the nozzle when pitch vectoring is included. For a ±15° nozzle pitch vectoring angle, the lower (or upper) trailing edge of the nozzle coincides with the lower (or upper) edge of the vane.

The external flow effects on the yaw vectoring produced by these three concepts are shown in figures 10 through 12. In these figures, the yawing moment multiplied by free-stream dynamic pressure is presented as a function of Mach number. It should be noted that for presentation purposes, the sign on yawing moment was changed from negative values (which would result from the positive flap deflections shown in figure 9) to positive values (which would result from negative flap deflections). On each of these figures, three pieces of data are presented. The circular symbols are the yawing moment based on the direct thrust contribution. These data were obtained from the yawing moment measured at static (wind-off) conditions multiplied by the ratio of the free-stream static to the free-stream dynamic pressure. The shaded area is the aerodynamic contribution of the vectoring device to the yawing moment measured by conducting the experimental test at jet-off conditions with external flow. The square symbols are the measured yawing moment at jet on conditions with external flow. The arrows shown in figures 10 to 12 indicate an induced external flow contribution to yawing moment caused by any interaction of the external flow with the jet-on vectored exhaust plume and any surrounding model surfaces. For the three cases presented in figures 10 through 12, the jet nozzle pressure ratio is 3.0. The yawing moment as a function of Mach number is presented for the upstream port in figure 10, for the sidewall flaps in figure 11, and for the post exit vanes in figure 12. For the upstream rectangular port configuration, the small flaps protruding from the side of the nozzles results in a small positive increment (aero. flap effect) in yawing moment which increases as the Mach number increases. The induced external flow contribution at jet on conditions, illustrated by the arrows, indicate that the external flow has an adverse contribution to the yawing moment. It is thought that this adverse effect could either be caused by the external flow altering the angle of the jet plume as it emanates from the side of the nozzle or by creating large negative pressures on the sidewall behind the jet plume. For the sidewall flap configuration (see figure 11), both the flaps themselves and the induced external flow contributions produced a positive increment in yawing moment. The increments are relatively small, which is expected since the flaps are small, and the deflection angle is only 20°. The largest external flow effects show up on the post- exit vane configuration (see figure 12). As shown, increasing Mach number causes large increases in the yawing moment obtained. The major portion of this increase is the result of a jet off aerodynamic effect on the vanes themselves. This is to be expected since the vanes are fairly large and protrude into the airflow, acting essentially like a vertical tail. A

summary of the thrust characteristics of these three nozzle concepts is presented in figure 13. In this figure the thrust minus nozzle drag divided by the ideal thrust is presented as a function of Mach number for the three nozzles at a yaw vector angle of 0° and 20°. For thrust vectored configurations reductions in this ratio form 1.0 are caused by the four following mechanisms: 1) skin friction, internal flow separation and exhaust flow divergence losses, 2) under-and over-expansion losses, 3) turning of the gross thrust vector away from the axial direction and 4) additional skin friction and pressure losses caused by the deployed thrust vectoring hardware and the actual turning process itself. The unvectored baseline configuration is affected by the first two mechanisms only. At a vector angle of 0°, the nozzle with the sidewall flaps and the upstream port exhibit the same performance which should be expected since neither has any additional exposed yaw vectoring hardware. However, adding the post-exit flaps causes a loss in performance due to the added skin friction and pressure drag of the external undeflected flaps. For the vectored case (right side of figure 13), the configuration with the sidewall flaps exhibits a thrust ratio very close to those for the unvectored nozzle. This result indicated that only a small loss occurs due to turning the exhaust flow for this yaw vector concept. The post-exit vane configuration exhibited a 5 percent lower thrust ratio than the unvectored nozzle concept and about 6 percent lower thrust ratio than the configuration with the sidewall flaps. The lower performance for this configuration probably results from supersonic exhaust flow separation (on the vane deflected away from the exhaust flow). The results for the upstream rectangular port configuration show extremely large thrust ratio losses. This loss is not surprising since about 30 percent of the flow does not pass through the main nozzle throat and thus is not efficiently expanded by the nozzle divergent flaps. In addition, this concept probably also has additional separation losses from the backside of the aft flap which extends into the internal exhaust stream.

Future civil transport aircraft must offer substantially improved performance at a lower operating cost if the viability of the commercial airlines is to be maintained. Accomplishing this task will require the development and application of many innovative and advanced technologies. With respect to airframe/propulsion integration, the objectives of this research is to eliminate any adverse interference penalties associated with the installation of the engines and even possibly developing methods of creating and taking advantage of any favorable interference effects. Key technology elements which will have a significant impact on the propulsion system integration characteristics for future aircraft and subsequently the performance and cost will be coupling of very high bypass ratio turbofan engines and/or counter rotating turboprop engines with advanced high aspect ratio supercritical wings. It is believed that with the proper integration of these propulsion technologies a 15 to 30 percent reduction in fuel consumption is possible. Incorporation of these technologies in conjunction with others such as laminar flow control, composite structures, and advanced control concepts indicate that the potential for even larger fuel savings are possible.

A number of airframe/propulsion integration studies related to turbofan engine integration have been conducted at the Langley Research Center (15). Form these studies the primary problem associated with integrating a nacelle/pylon/wing can be established. For example in reference 16 the results of a study on a high wing transport model representative of a STOL aircraft concept is presented. A photograph of this model is presented in figure 14. The wing of this model has an aspect ratio of 7.52 and a quarter-chord sweep angle of 30°. An axisymmetric long-duct flow through nacelle was mounted in a conventional location at a semispan station of 0.328. As illustrated in figure 15, the nacelle/pylon significantly changes the wing pressure distribution at a $M = 0.80$ particularly around the wing leading edge. The velocity increases on the wing lower surface reducing the lift on the wing and altering the wing span load distribution thereby increasing the wing drag due to lift which shows up as an unfavorable interference effect. Reducing this unfavorable effect therefore can be accomplished by reducing these local velocity increases. The rest of this section on turbofan aircraft will concentrate on reducing or eliminating these unfavorable velocity perturbations. According to the data presented in figure 16, the major part of the unfavorable effects is caused by the pylon and not by the nacelle/pylon combination. As shown in this figure, essentially all of the lift loss is due to adding the pylon as well as the larger portion of the drag. The drag increase at cruise lift for the nacelle/pylon combination is probably attributed to the skin friction drag of the long duct nacelles. In view of these results NASA undertook a study using the model in figure 14 to investigate various plyon shapes (no engine nacelle required) on the wing pressure distributions.

In this study (described in reference 17) several pylon shapes were studied including plyon contoured to the shape of the streamlines of the local flow on the undersurface of the wing and a second series called compression pylons. These pylons increased linearly in thickness along the chord with the maximum thickness occurring at the wing trailing edge station. That means that all of the pylon closure was achieved behind the wing trailing edge. A photograph of the high wing transport model with 12 percent thick compression type pylon is presented in figure 17. This pylon was located at a semispan station of 0.39 with its leading edge located at the wing leading edge and its maximum thickness station at the wing trailing edge. The pressure coefficient data measured inboard of the pylon for several pylons are presented in figure 18. As indicated previously, the flow accelerates around the pylon/wing juncture for the conventional pylon causing the loss in lift on wing lower surface. The compression pylon eliminates this velocity increase (solid symbols) such that the pressure coefficient distribution for the wing with the compression pylon is very similar to the pressure coefficient distribution for the wing alone.

An alternate nacelle integration arrangement which tends to exhibit much the same effect as the compression pylon is shown in figure 19. This nacelle is mounted to the undersurface of the wing such that the inlet is located at a 70 percent wing chord station (see ref. 15). The aerodynamic characteristics also presented in this figure show that adding the nacelle results in an increase in lift coefficient instead of the decrease noted for the conventional engine nacelle arrangement. This lift increase results in a reduction in the drag due to lift. In fact, for this engine installation favorable interference is achieved. That is, the nacelles were added such that the resulting additional drag was less than the skin friction drag attributed to the nacelles.

Several new models have been considered during the past few years to more closely match the evolving aircraft proposals from the various companies. One of these models, designed in 1983–85 and constructed in 1986-88, was tested in the Langley 16-Foot Transonic Tunnel in January and March of 1989. Figure 20 is a photographic of the 1/17-scale, supercritical airfoil, low-wing transport model taken from reference 18. It represents a 150 passenger, twin-engine transport with design cruise Mach number of 0.77, has a wing quarter chord sweep angle of 21°, and a wing aspect ratio of about 10.8. Since only the interference effects of the nacelles on the wing and vice versa were being studied, no attempt was made to add tail surfaces to the model. Instead, a simple afterbody was used to fair into the base surrounding the model support sting. A six-component strain gage balance located on the fuselage centerline near the quarter chord of the wing mean aerodynamic chord was used to measure aerodynamic forces and moments on the model.

In this study several advanced nacelle designs were studied. One of them shown in the photograph was a flow-through nacelle representing a very high bypass ratio (BPR $\approx$ 20) or superfan nacelle. It was expected that because of the large size of this nacelle the adverse interference drag would be significant. However, in the design process the local areas around the pylon wing juncture was carefully tailored in order to avoid the large

velocity increases. As you can see from the data presented in figure 21, where the increment in drag due to the nacelle is shown as a function of lift coefficient, the increment associated with the nacelle is slightly less than the skin friction drag of the nacelles. This means that with careful design the adverse interference drag can be eliminated.

The recent world wide fuel crisis caused a significant level of interest in developing new technologies for decreasing fuel consumption. One of the most significant new technologies under study is related to the integration of advanced high speed turboprop engines. NASA's Langley Research Center is conducting studies which are aimed at developing an understanding the flow interactions associated with turboprop integration; obtaining detailed pressure for use in code validation; and the aerodynamic integration characteristics for conventional and unconventional aircraft concepts.

Since the goals of this study were to develop an understanding of the basic flow characteristics, the study was comprised of a straight wing and a swept wing both having the same chord length and the same isolated wing pressure distribution. A photograph of the straight wing model with a single rotation turboprop installation is presented in figure 22. The basic flow interactions for this straight wing/turboprop model is presented in figure 23. The wing pressure coefficient data for two stations is shown, one for the upwash side of the propeller (left side or figure) and the other for the downwash side. From these data it is easy to determine the integration problems that will be encountered in designing a transport aircraft. For example, these data show that adding the nacelle (without the propeller) causes a flow acceleration over the surface of the wing. However, adding the propeller with its thrust effects and swirling flow causes an increase in lift on the upwash side of the propeller and a significant decrease in lift on the downwash side. This means that to properly integrate the nacelles with the wing may require a wing design that is different for the right and left sides of the aircraft (assuming a twin engine aircraft with single rotation propellers).

The results of a study aimed at integrating a counter rotating propeller onto a swept wing configuration is presented in figure 24. This study will illustrate some of the configuration modifications which have to be considered to properly integrate a turboprop engine. This study used a model of an advanced 150 passenger transport and was conduced with the aid of a computational method developed for NASA Langley Research Center by the Boeing Company. A sketch of the basic wing with a symmetrical nacelle is presented on the right side of this figure as the solid line. The Euler code was used to predict the pressure distributions over the wing at a station just inboard of the nacelle and the results are presented in this figure. The straight nacelle/wing combination caused a significant increase in velocities on the wing upper surface which probably resulted in a fairly strong shock wave and its accompanying high wave drag and the potential for flow separation. Several modifications were studied with this code. These included, as illustrated by the configuration represented by the dashlines, a leading-edge strake on the inboard portion of the wing and some local contouring of the nacelle. This contouring was accomplished by calculating a local flow streamline over the wing and wrapping the nacelle evenly around the streamline. The pressure distribution for the model with these modifications is presented also in figure 24 and show that the high velocities over the wing have been significantly reduced. Similar modifications made on a model with an underwing nacelle were very effective in reducing the installation drag.

In addition to the relatively conventional turboprop installations that have been under study, a fairly sizable effort has been devoted to unconventional concepts which may offer the potential for significant performance increases. One such configuration shown in figure 25 is the wing tip turboprop model (see reference 19). In undertaking this program, it was felt that a propeller located behind the wing trailing edge at the wing tip in the cross flow of the wing tip vortex could possibly recover part of the vortex energy as an increase in propeller thrust. Additionally, using the propeller wake to disrupt the wing vortex system could result in a reduction in the lift induced drag as well. The results of this study conducted in NASA Langley's 7- by 10-Foot High-Speed Tunnel at a Mach number of 0.70 are also represented in figure 25.

The effect of the wing-tip mounted pusher turboprop on drag is shown on this figure where drag coefficient is presented against lift coefficient. At zero lift coefficient, where no vortex exists, the measured drag coefficient for the configuration, with a propeller pitch angle of 57.1°, is equal, approximately, to the wing along drag plus the skin friction drag of the turboprop nacelle (calculated flat plate skin friction drag of the nacelle based on a $C_f = 0.0035$). The reduction in induced drag obtained by the pusher turboprop/vortex interaction is approximately 30 percent of the induced drag of the wing alone adjusted drag at $C_L = 0.35$.

CONCLUSIONS

A significant research program is ongoing at NASA's Langley Research Center on integrating the propulsion system with the aircraft. This program has included nacelle/pylon/wing integration for turbofan transports, propeller/nacelle/wing integration for turboprop transports and nacelle/afterbody empennage for high performance aircraft. The results indicate the following:

1. A significant portion of the afterbody drag is due to the horizontal and vertical tails.
2. Thrust vectoring concepts are effective in providing combined pitching and yawing moments.
3. Careful contouring of the pylon/wing and nacelle/wing for transport aircraft is required if the adverse interference effects are to be eliminated.
4. Advanced configurational concepts have shown the potential for significant performance increases.

REFERENCES

1. Flectcher, J.; and Burns, B. R. A.: "Supersonic Combat Aircraft Design," AIAA Paper No. 79-0699, March 1979.
2. Nichols, Mark R.: "Aerodynamics of Airframe-Engine Integration of Supersonic Aircraft," NASA TND-3390, 1966.
3. Corson, Blake W., Jr.; and Runckel, Jack F.: "Exploratory Studies of Aircraft Afterbody and Exhaust-Nozzle Interaction," NASA TN X-1925, 1969.
4. Runckel, Jack F.: "Interference Between Exhaust System and Afterbody of Twin-Engine Fuselage Configurations," NASA TN D-7525, 1974.
5. Glasgow, E. R.; and Santman, D. M.: "Aft-End Design Criteria and Performance Prediction Methods Applicable to Air Superiority Fighters Having Twin Buried Engines and Dual Nozzles," AIAA Paper No. 72-1111, Nov.–Dec. 1972.
6. Glasgow, E. R.: "Integrated Airframe Nozzle Performance for Designing Twin-Engine Fighters," AIAA Paper No. 73-1303, November 1973.
7. Berrier, B. L.: "Empennage/Afterbody Integration for Single and Twin Engine Fighter Aircraft," AIAA Paper No. 83-1126, 1983.
8. Leavitt, Laurence D.: "Effect of Various Empennage Parameters on the Aerodynamic Characteristics of a Twin-Engine Afterbody Model," AIAA Paper No. 83-0085, 1983.
9. Berrier, Bobby L.: "Effect of Empennage Interference on Single-Engine Afterbody/Nozzle Drag," AIAA Paper No. 75-1296.
10. Burley, James R.; and Berrier, Bobby L.: "Investigation of Installation Effects on Single-Engine Convergent-Divergent Nozzles," NASA TP-2078, November 1982.

11. Henderson, William P.; and Burley, James R., II: "Effect of Empennage Arrangement on Single-Engine Nozzle/Afterbody Static Pressures at Transonic Speeds." NASA TP-2753, November 1987.

12. Putnam, Lawrence E.; and Bissinger, N. C.: "Results of AGARD Assessment of Prediction Capabilities for Nozzle Afterbody Flows," AIAA Paper No. 85-1464, July 1985.

13. Burley, James R.; and Berrier, Bobby L.: "Effect of Tail Span and Empennage Arrangement on Drag of a Typical Single-Engine Fighter Aft End," NASA TP-2352, September 1984.

14. Berrier, Bobby L.; and Re, Richard J.: "A Review of Thrust-Vectoring Schemes for Fighter Applications," AIAA Paper No. 78-1023, July 1978.

15. Henderson, William P.; and Patterson, James C., Jr.: "Propulsion Installation Characteristics for Turbofan Transports," AIAA Paper No. 83-0087, 1983.

16. Lee, Edwin F., Jr.; and Pendergraft, Odis C., Jr.: "Installation Effects of Long-Duct Pylon—Mounted Nacelles on a Twin-Jet Transport Model with Swept Supercritical Wing," NASA TP-2457, 1985.

17. Carlson, John R.; and Lamb, Milton: "Integration Effects on Pylon Geometry and Rearward Mounted Nacelles for a High-Wing Transport," AIAA Paper No. 87-1920, 1987.

18. Pendergraft, Odis C., Jr.; Ingraldi, Anthony M.; Re, Richard J.; and Kariya, Timmy T.: "Nacelle/Pylon Interference Study on a 1/17th-Scale, Twin-Engine, Low-Wing Transport Model," AIAA Paper No. 89-2480, 1989.

19. Patterson, James C., Jr.; and Bartlett, Glynn R.: "Effect of a Wing-Tip Mounted Pusher Turboprop on the Aerodynamic Characteristics of a Semi-Span Wing," AIAA Paper No. 85-1347, 1985.

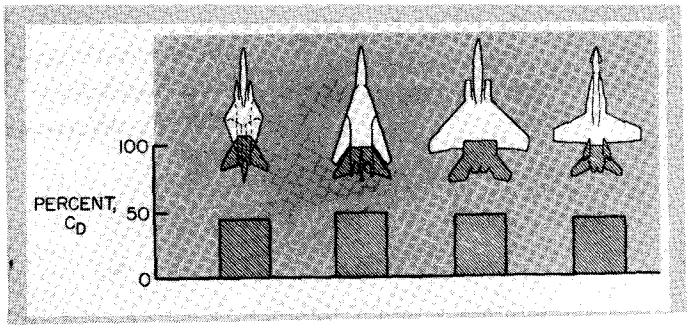

Figure 1. - Propulsion Integration Characteristics for High Performance Aircraft.

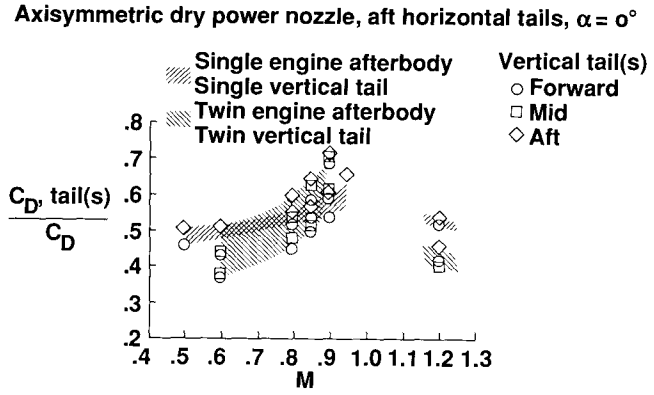

Figure 2. - Effect of Empennage on Afterbody Drag.

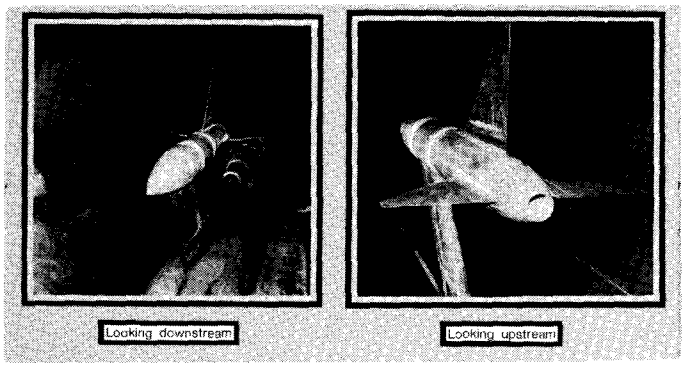

Figure 3. - Single - Engine Configuration in the Langley 16 - Foot Transonic Tunnel.

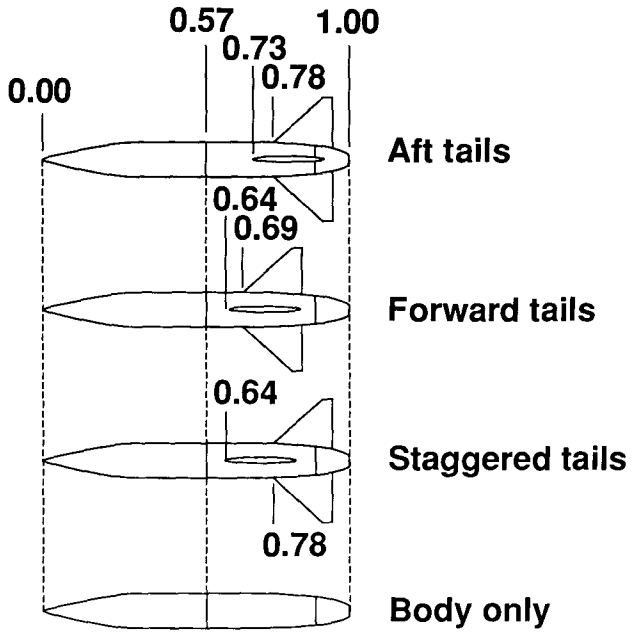

Figure 4. - Empennage Arrangements Studied.

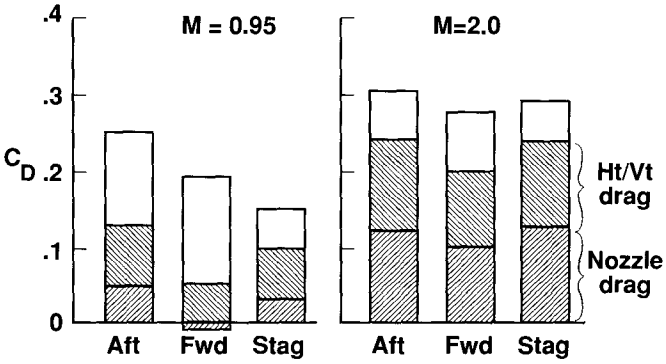

Figure 5. - Effect of Empennage Arrangement on Nozzle/Afterbody Drag. NPR = Scheduled.

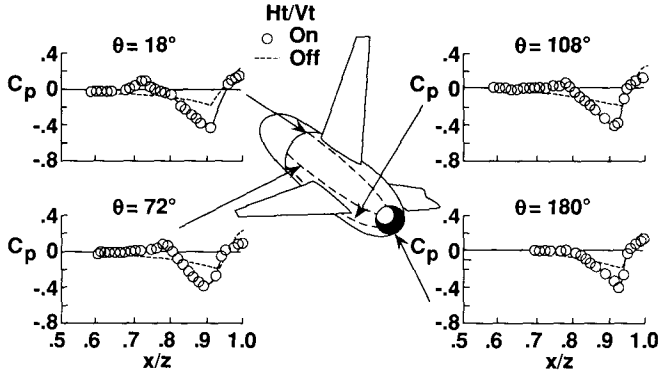

Figure 6. - Effect of Empennage on Afterbody Pressures. M = 0.95, NPR = 3.02.

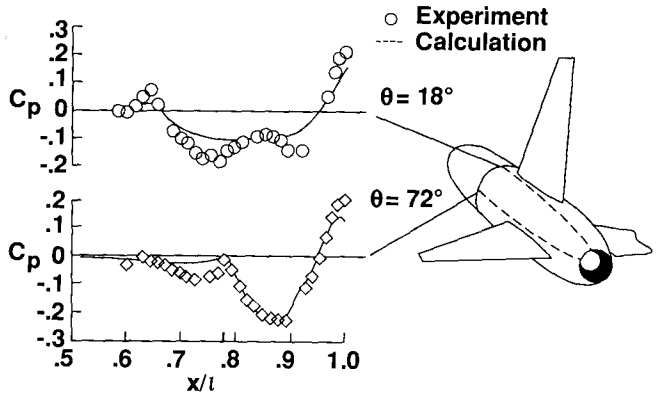

Figure 7. - Comparison of Experimental and Theoretical Pressure Coefficients. M = 0.90, NPR = 5.0.

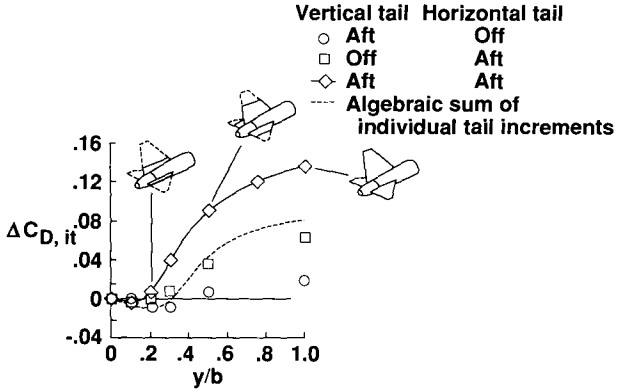

Figure 8. - Effect of Tailspan on Interference Drag. M = 0.95, NPR = 3.97.

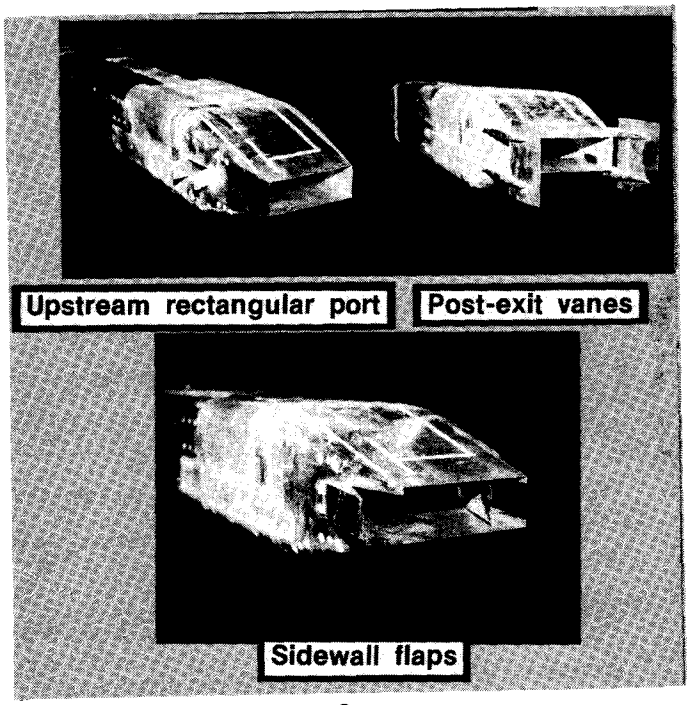

Figure 9. - Yaw Vector Concepts.

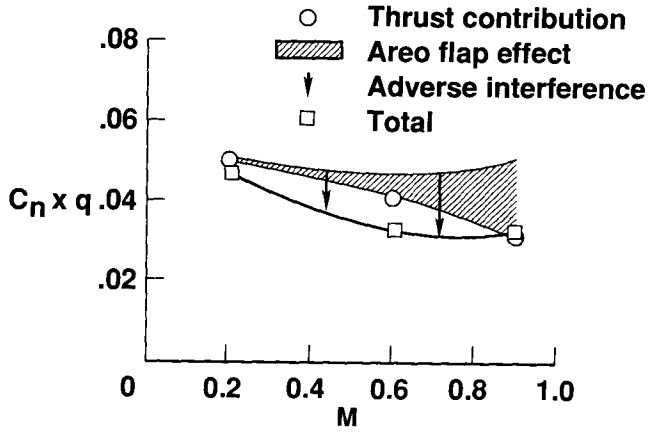

Figure 10. - External Flow Effects on Yawing Moment. Upstream Rectangular Port Concept. α = 0°, δv,y = 19.6°, δv,p = 0°, NPR = 3.0.

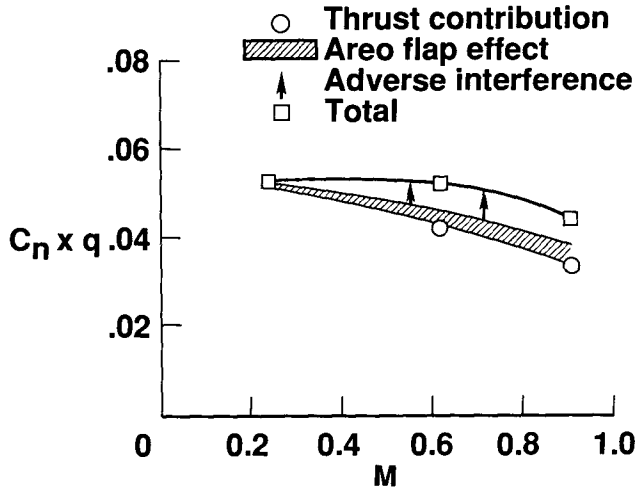

Figure 11. - Internal Flow Effect on Yawing Moment. Sidewall Flap Concept. α = 0°, δv,y = 20°, δv,p = 0°, NPR = 3.0.

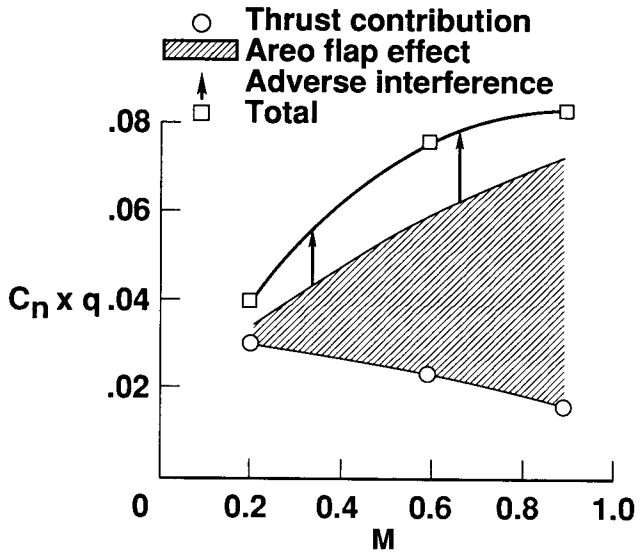

Figure 12. - External Flow Effects on Yawing Moment. Post - exit Vane Concept. $\alpha = 0°$, $\delta v,y = 20°$, $\delta v,p = 0°$, NPR = 3.0.

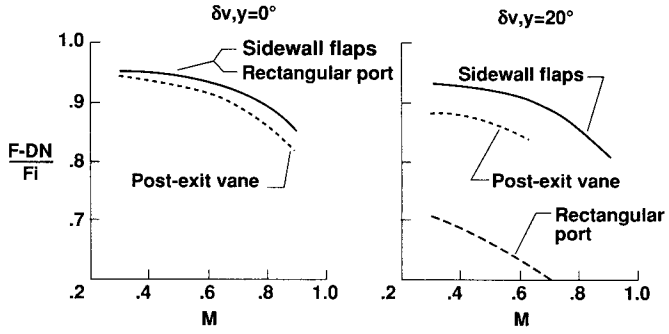

Figure 13. - Effect of Yaw Vectoring Concepts on Thrust Performance.

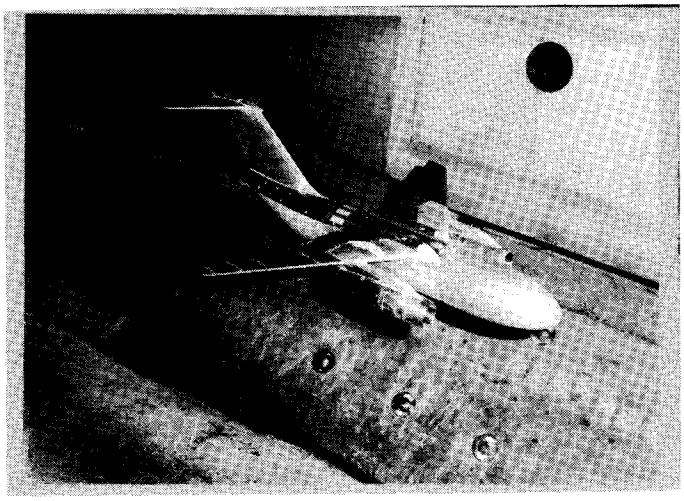

Figure 14. - High Wing Transport in the 16-Foot Transonic Tunnel.

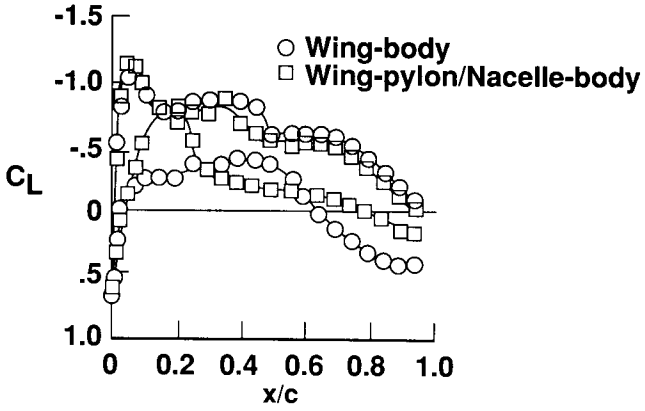

Figure 15. - Effect of Engine Nacelle/Pylon on Wing Pressure Distributions. M = 0.80, $\alpha = 1.24°$, y/b/2 = 0.328.

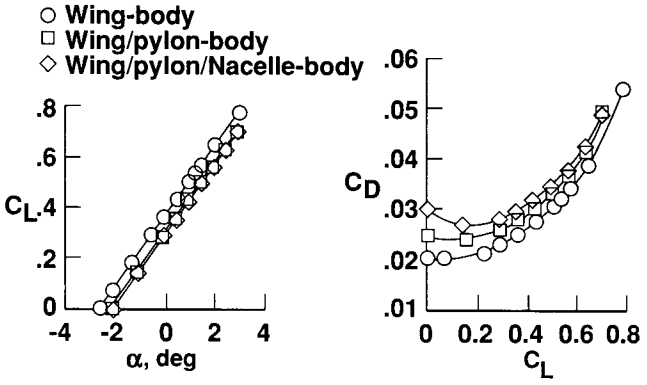

Figure 16. - Effect of Engine Nacelle/Pylon on Lift and Drag Characteristics. M = 0.80.

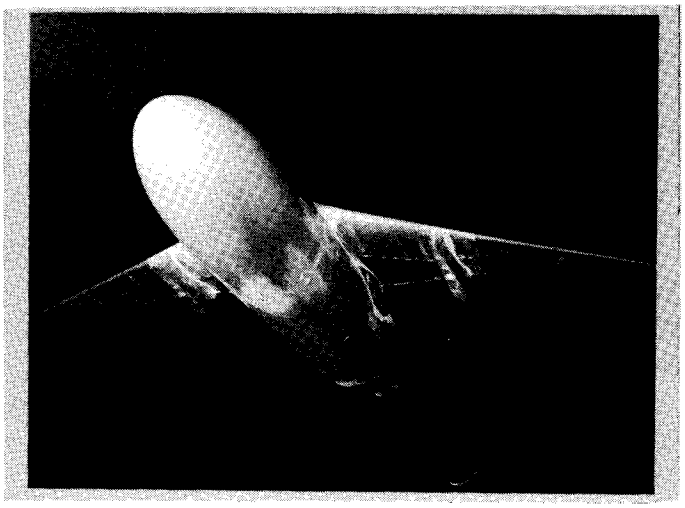

Figure 17. - Photograph of Model with Compression Pylons.

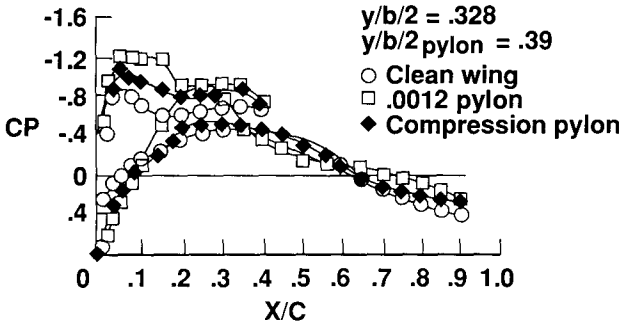

Figure 18. - Effect of Pylon Shapes on Wing Pressure Distributions. M = 0.80, $C_L \approx 0.50$.

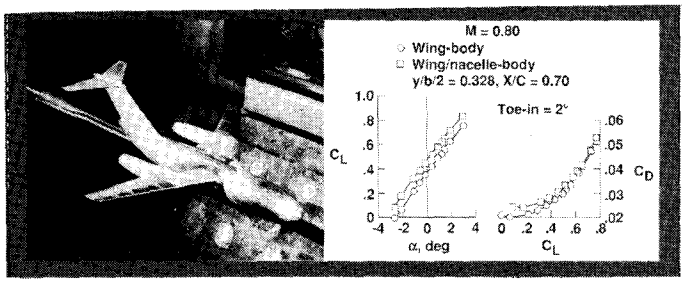

Figure 19. - Effects of Wing Aft-mounted Nacelles on the Lift and Drag Characteristics.

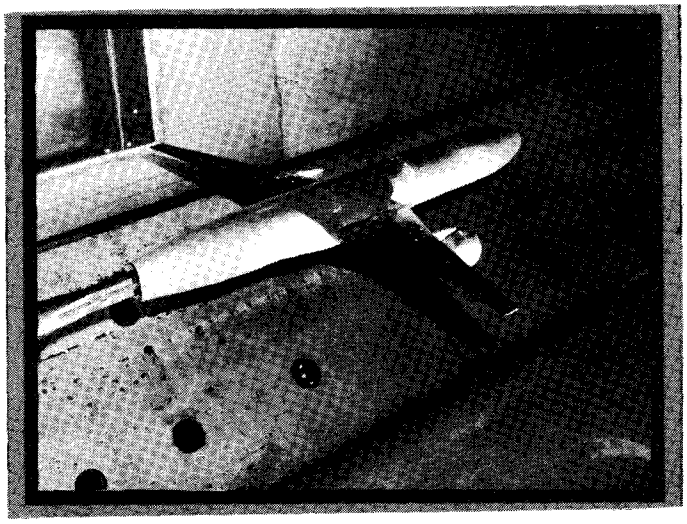

Figure 20. - Low Wing Transport with High Bypass Ratio Nacelles in Langley 16-Foot Transonic Tunnel.

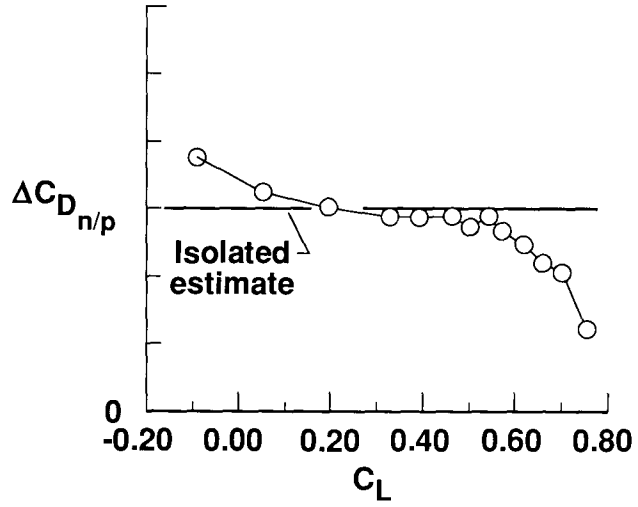

Figure 21. - Drag Increment Due to Nacelle/Pylon. M = 0.77.

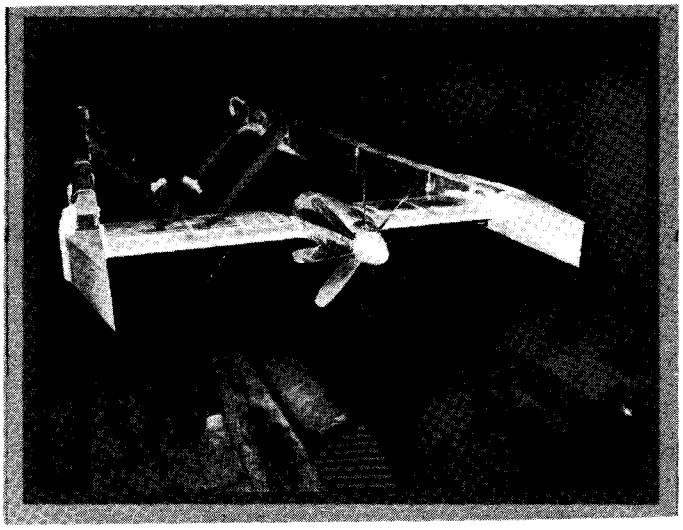

Figure 22. - Turboprop Integration Model in the Langley 16-Foot Transonic Tunnel.

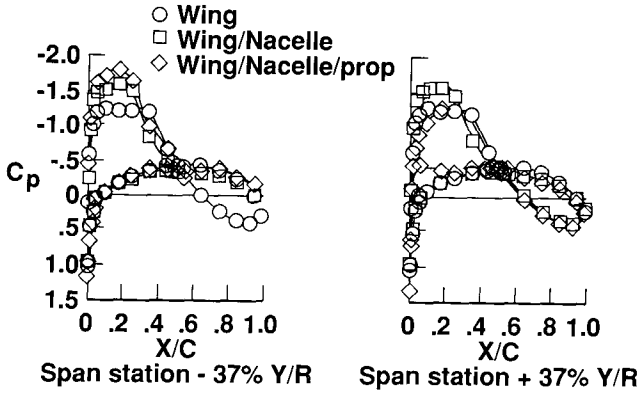

Figure 23. - Effect of Propeller Rotation on Wing Pressure Distributions. M = 0.77, $\alpha = 3°$, $C_T = 0.392$, J = 3.24.

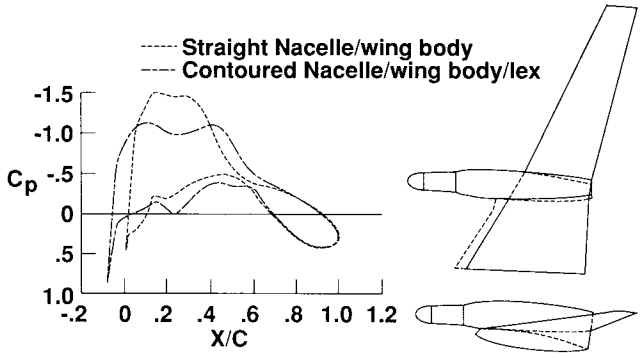

Figure 24. - Effect of Nacelle Shape on Wing Pressure Distributions. M = 0.77, C_L = 0.55, y/b/2 = 0.35.

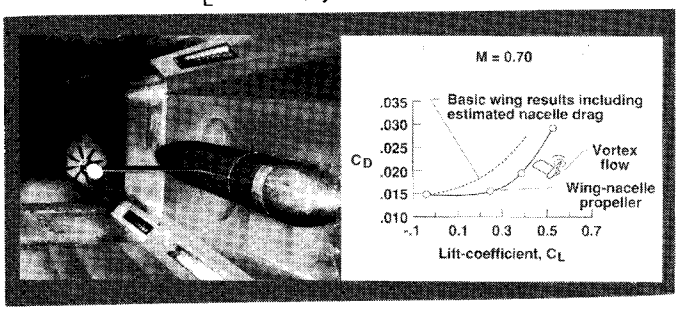

Figure 25. - Effect of Wing-tip Mounted Turboprop on the Drag Characteristics.